PROPULSION SIMULATIONS WITH THE UNSTRUCTURED-GRID CFD TOOL *TetrUSS*

Karen A. Deere[†]
Aerodynamics, Aerothermodynamics and Acoustics Competency
NASA Langley Research Center, Hampton, Virginia

Dr. Mohagna J. Pandya[*]
Swales Aerospace, Hampton, Virginia

ABSTRACT

A computational investigation has been completed to assess the capability of the NASA *Tetra*hedral *U*nstructured *S*oftware *S*ystem *(TetrUSS)* for simulation of exhaust nozzle flows. Three configurations were chosen for this study: (1) a fluidic jet effects model, (2) an isolated nacelle with a supersonic cruise nozzle, and (3) a fluidic pitch-thrust-vectoring nozzle. These configurations were chosen because existing data provided a means for measuring the ability of the *TetrUSS* flow solver USM3D for simulating complex nozzle flows. Fluidic jet effects model simulations were compared with structured-grid CFD data at Mach numbers from 0.3 to 1.2 at nozzle pressure ratios up to 7.2. Simulations of an isolated nacelle with a supersonic cruise nozzle were compared with wind tunnel experimental data and structured-grid CFD data at Mach numbers of 0.9 and 1.2, with a nozzle pressure ratio of 5. Fluidic pitch-thrust-vectoring nozzle simulations were compared with static experimental data and structured-grid CFD data at static freestream conditions and nozzle pressure ratios from 3 to 10. A fluidic injection case was computed with the third configuration at a nozzle pressure ratio of 4.6 and a secondary pressure ratio of 0.7. Results indicate that USM3D with the S-A turbulence model provides accurate exhaust nozzle simulations at on-design conditions, but does not predict internal shock location at overexpanded conditions or pressure recovery along a boattail at transonic conditions.

INTRODUCTION

Unstructured-grid (USG) methodology has matured through the 1990's as a productive computational fluid dynamics (CFD) tool for rapid aerodynamic analysis and design of complex configurations. Its primary benefit is derived from a reduced turnaround time for generating CFD solutions in a matter of days, rather than weeks or months with conventional structured-grid technology. Such benefit is enabled by discretizing the domain with tetrahedral cells, which can be easily generated around the most complex of configurations using the VGRID code (ref 1). Key components of the USG methodology have been consolidated into a user-friendly flow analysis tool called the NASA *Tetra*hedral *U*nstructured *S*oftware *S*ystem (*TetrUSS*) (ref. 2). To date, most applications of *TetrUSS* have addressed external flow problems. The present work initiates an investigation of its applicability to propulsion simulation problems.

Computational assessment of propulsion applications, and more specifically fluidic thrust vectoring (FTV) nozzles, generally requires the use of higher-level turbulence models to adequately model complex flow features (refs. 3-5). The introduction of a secondary air stream into a primary jet flow of a nozzle can shift the sonic plane, create shocks in supersonic flow, and cause regions of separated flow. These features, as well as exhaust flow shear layers, can be challenging to predict.

Structured-grid CFD codes such as PAB3D (ref. 6), CFL3D (ref. 7), OVERFLOW (ref. 8) and TLNS3D (ref. 9) have long supported 2-equation turbulence models, some with Algebraic Reynolds Stress Models (ARSM), to capture complex flow structures. One-equation models and wall functions do not appear to be adequate enough for simulating exhaust nozzle flows at off-design conditions.

While the predominant turbulence model in many unstructured-grid codes is the Spalart-Allmaras (S-A) 1-equation model, progress is being made toward adapting 2-equation models to these codes. Reference 10 reports progress toward implementing two k-ε turbulence models and the Girimaji non-linear ARSM higher-level turbulence models into the flow solver, USM3D, which

---

[†] Aerospace Engineer, Configuration Aerodynamics Branch, Senior Member AIAA
[*] Senior Research Engineer, Member AIAA

is a component of the *TetrUSS* system. Preliminary code assessments with a flat plate, an airfoil, and a wing configuration indicate improved skin friction prediction on the flat plate and improved transonic shock location prediction on the airfoil and wing with the Carlson modified k-ε turbulence model (ref. 10). As accurate unstructured-grid CFD methods become available for propulsion applications, the design and analysis time of exhaust nozzles will be dramatically decreased. Additionally, many geometric configurations too complex for structured-grid generation could be evaluated with unstructured-grid simulations.

As the development and improvement of the higher-order turbulence models in USM3D continues, the current work begins an assessment of the TetrUSS flow analysis system for propulsion simulations and creates a baseline set of solutions using the S-A 1-equation turbulence model. Three exhaust nozzles are analyzed. Initially, three-dimensional external and internal flow simulations were completed on the fluidic pitch-thrust-vectoring nozzle investigated in reference 5. Subsequently, three-dimensional external and internal flow simulations were completed on an isolated nacelle with a nozzle designed for the supersonic cruise civil transport (ref. 11). Finally, three-dimensional internal flow simulations were completed on the fluidic pitch-thrust-vectoring nozzle investigated in reference 12. Results are compared with measured experimental data and with data from the structured-grid flow solver PAB3D, using advanced 2-equation, linear and nonlinear, turbulence models. This work will provide the foundation for continued code validation of the advanced turbulence models as they become available in USM3D.

NOMENCLATURE

ARSM	algebraic Reynolds stress model
A_e	nozzle exit area
A_t	nozzle throat area
A_e/A_t	expansion ratio
a	geometric scaling parameter, prefer a<0.5
nLayer	number of prismatic cells normal to the body in the boundary layer grid
b	growth parameter, 0.07 used for all grids
C_p	pressure coefficient, $(p-p_\infty)/(0.5\rho U^2)$
FJEM	fluidic jet effects model
FPVN	fluidic pitch-thrust-vectoring nozzle
k	turbulent kinetic energy
L	reference length
M	Mach number
NPR	nozzle pressure ratio, $p_{t,jet}/p_\infty$
p	local static pressure
$p_{o,jet}$	normalized total pressure, equation 2
$p_{t,jet}$	jet total pressure
$p_{t,j}$	jet total pressure
p_{jet}	jet static pressure
$p_{t,slot}$	secondary flow total pressure
p_∞	free stream static pressure
R	radius of curvature
SCN	isolated nacelle with supersonic cruise nozzle
SPR	secondary pressure ratio, $p_{t,slot}/p_{t,jet}$
3D	three-dimensional
2DCD	two-dimensional, convergent-divergent
T_∞	freestream static temperature
$T_{o,\infty}$	freestream total temperature
$T_{o,jet}$	normalized total temperature, equation 4
$T_{t,jet}$	jet total temperature
U	freestream velocity
x	axial distance
y^+	nondimensional first cell height
Δz_1	dimensional first cell height
ε	turbulent energy dissipation
γ	ratio of specific heat
ρ	density

THREE CONFIGURATIONS

I. Fluidic Jet Effects Model (FJEM)

The first configuration used for the current study was a two-dimensional, convergent-divergent (2DCD) fluidic thrust-vectoring nozzle, which was installed in an isolated nacelle to investigate the interaction between the external freestream flow and the nozzle exhaust flow (ref. 5). An isometric view of the isolated nacelle mounted on a strut is shown in figure 1. However, the strut was not modeled in either the current or the previous investigation. In addition, secondary fluidic injection for pitch vectoring was not simulated in the current study.

The length of the isolated nacelle was L=64.745 inches. The nozzle length was 8 inches, the throat area was A_t=5.416 in.^{2}, and the expansion ratio was A_e/A_t=2.4. The design nozzle pressure ratio (NPR_D) and exit Mach number, based on one-dimensional theory, were NPR_D=14.588 and M=2.4, respectively. Structured and unstructured grids along the Symmetry plane of the isolated nacelle and nozzle are shown in figures 2 (a) and (b), respectively.

Four unstructured, tetrahedral grids were generated with VGRID, one for each Mach number listed in Table 1. The tetrahedral cell count for the half plane geometry and the parameters for generating the boundary layer grid are also shown in Table 1. To ease grid generation with VGRID, the 0.02-inch thick trailing edge was modified to a sharp trailing edge. This modification was also made in the structured grid. The sharp edge was created by extending the 10° boattail surface until it intersected an extension of the internal divergent wall. This

geometry modification shifted the exit from x=43.345 inches to x=43.396 inches. The nose of the nacelle was located at x=-21.4 inches. The upstream and downstream boundaries were located five reference lengths (5*L*), and the lateral boundaries were located 3*L*, away from the nacelle. The size of the largest cells along the far walls of the domain, were determined in VGRID by dividing the domain length by 25. This strategy puts approximately 25 tetrahedra along the length of the domain. The cells along the nacelle nose and centerbody were stretched to reduce the total number of cells. A maximum stretching ratio of 6:1 was used at the nacelle midbody. The cells inside the nozzle and along the boattail were not "stretched" because these areas were the focus of this study.

Simulations were computed with freestream Mach numbers of *M*=0.3, 0.7, 0.9, 1.2 and nozzle conditions of NPR=3.6, 5, 6, 7.2, respectively.

M	y^+	a	Δz_1 (in.)	nLayer	viscous cells	total cells
0.3	2	0.2244	0.33e-3	16	1,206,411	2,120,799
0.7	2	0.2504	0.154e-3	16	1,223,463	2,160,582
0.9	2	0.2583	0.123e-3	16	1,228,995	2,167,318
1.2	2	0.2674	0.949e-4	16	1,236,270	2,177,580

Table 1. Tetrahedral cell count and boundary layer grid parameters for FJEM.

II. Isolated Nacelle with Supersonic Cruise Nozzle (SCN)

The second configuration (fig. 3(a)) used in the current study was an isolated nacelle with a nozzle designed for the supersonic cruise civil transport. This configuration was tested in the 16-Foot Transonic Tunnel at NASA Langley Research Center and was simulated with the structured-grid CFD code, PAB3D, to determine the effects of geometric variations on nozzle drag (ref. 11).

The length of the isolated nacelle was *L*=64.04 inches. Flap 1 and sidewall 1 were chosen from reference 11 for this study. The flap along the boattail had an angle of 16.38° with a 40 percent radius of curvature and the sidewall angle was 4° with a sharp corner. The nozzle length was 13.14 inches, the throat area was A_t=11.09 in.^{2}, and the expansion ratio was A_e/A_t=1.34. The design nozzle pressure ratio and exit Mach number, based on one-dimensional theory, were NPR_D=5 and *M*=1.7, respectively. The symmetry plane and surface geometry for the unstructured grid are shown in figures 3 (b) and (c), respectively.

The tetrahedral cell count for the quarter plane geometry and the parameters for generating the boundary layer grid are shown in Table 2. The upstream and downstream boundaries were located 5*L*, and the lateral boundaries were located 3*L*, away from the nacelle. Approximately 25 tetrahedra were used along the length of the domain. The cells along the nacelle nose and centerbody were stretched to reduce the total number of cells. A maximum stretching ratio of 2.7:1 was used at the transition from the nose to centerbody geometry. The cells were not "stretched" inside the nozzle or along the boattail because this was the main region of interest. The sidewall trailing edge source was moved upstream 0.04 inches, off the surface, to eliminate invalid vectors that appeared during grid generation with the source on the trailing edge surface.

The fine nozzle grid (listed in Table 2) had cells half the size of the baseline grid inside the nozzle. In addition, the fine nacelle grid also had less stretching along the nacelle. The fine nacelle surface grid was also used to generate a grid with a y^+=50 for simulations with a wall.

Simulations were computed at the design NPR of 5 with an external freestream flow of *M*=0.9 and 1.2.

Name	y^+	a	Δz_1(in.)	nLayer	viscous cells	total cells
Baseline	2	0.266	0.24e-5	16	124,602	686,306
Fine Nozzle	2	0.266	0.24e-5	16	334,581	1,477,890
Fine Nacelle	2	0.266	0.24e-5	16	603,816	1,512,986
Fine Nacelle	50	0.232	0.93e-4	12	434,724	1,320,777

Table 2. Tetrahedral cell count and boundary layer grid parameters for SCN.

III. Fluidic Pitch-Thrust-Vectoring Nozzle (FPVN)

The third configuration used for the current study was a 2DCD fluidic pitch thrust-vectoring nozzle, which was tested at the NASA Langley Jet Exit Test Facility at static (wind-off) conditions and was simulated with the structured-grid CFD code, PAB3D (ref. 12).

The nozzle length was 4.55 inches, the throat area was A_t=4.328 in.^{2}, and the expansion ratio was A_e/A_t=1.7098. The design nozzle pressure ratio and exit Mach number, based on one-dimensional theory, were NPR_D=8.78 and *M*=2.075, respectively. The internal nozzle geometry of the upper wall and the location of the injection slot are shown in figure 4(a).

The tetrahedral cell count for the half plane geometry and the parameters for generating the boundary layer grid are shown in Table 3. Static internal nozzle performance was the primary interest for this case, so the external freestream geometry was not modeled with a smooth, full nacelle shape, like the previous cases. The far field boundary was located at 2*L* upstream of the nozzle. This boundary did not need to be located very far upstream since the freestream was modeled with near static conditions, *M*=0.1. The external trailing edge was modified to fit the plenum inside the geometry, compare figures 4(b) and 4(c). This modification was expected to have negligible impact on nozzle flow with

a static freestream flow. In fact, this geometry was more representative of the experimental nozzle hardware, see figure 4(a).

Simulations were computed at NPR from 3 to 10 with static freestream conditions (M=0.1). A fluidic injection case was computed at NPR=4.6 with a secondary to primary total pressure ratio of SPR=0.7

Name	y^+	a	Δz_1(in.)	nLayer	viscous cells	total cells
Baseline1	1	0.29	2.3e-5	15	786,498	1,158,098
Baseline2	.18	0.28	0.4e-5	18	885,228	1,261,251
Injection	1	0.29	2.3e-5	17	1,121,307	1,545,405

Table 3. Tetrahedral cell count and boundary layer grid parameters for FPVN.

COMPUTATIONAL STUDY

Grid Generation

The unstructured grid generation process began with a tool called, GridTool. The geometry of interest can be read into GridTool using IGES, GRIDGEN, PLOT3D, LaWGS, or curves file format. The geometry can also be "drawn" directly in GridTool. The user generates patches on the surface geometry, adds sources that will define cell size, specifies layer parameters that define the grid characteristics in the boundary layer, and writes out a file for the grid generator, VGRID. At this point, grid generation becomes automated. VGRID generates a thin boundary layer (if viscous simulation is desired) using the advancing layers method and fills the inviscid domain with tetrahedral cells using the advancing front method. More details of the grid generation process are described references 1 and 13. The grid is "completed" using POSTGRID, which fills in any pockets of void space where VGRID was not able to generate cells. The unstructured grid utility program, usgutil, aids the user in defining boundary layer parameters, mirroring grid files, performing file conversion, and extracting data. The unstructured codes and tools noted above allow for a nearly automated grid generation process of complex grid generation in days, compared to weeks for structured grid generation. Approximate grid generation times for the three configurations used in this study are shown in Table 4. The FJEM structured grid was generated by an expert CFD user in 1997, which required a major modification to the AXB code. One could argue that structured grid generation has improved over the last 5 years. While this is true, recent structured grids generated by experts in GEOLAB at NASA Langley have still taken 10 days for a three dimensional (3D) dual-stream chevron nozzle with a pylon, and months for a complex 3D internal nozzle, with flaps and slots.

For some users, a potential draw back to the unstructured-grid generation method is the definition of a single boundary layer grid for the entire geometry. For the current study, boundary layer grid definitions for a range of conditions, inside the nozzle and along the external nacelle, were investigated. The most stringent boundary layer grid definition was used for the entire surface. Although this method will provide adequate grid resolution where needed, it may also produce more grid points than necessary in certain locations. For example, if the first cell height in the boundary layer is smallest inside the nozzle, the definition to provide adequate y^+ in this region will be more than sufficient along the nacelle. Without the ability to define more than 1 boundary layer, the grid will be larger than required. Therefore, more memory will be required than if two or more boundary layer definitions could have been defined.

Geometry	Unstructured	Structured
FJEM-3D	2	30
SCN-3D	5	17
FPVN-2D	2	4

Table 4. Estimate of grid generation time in days.

Governing Equations

USM3D (refs. 14-15) is a tetrahedral cell-centered, finite volume Euler and Navier-Stokes (N-S) flow solver. Inviscid flux quantities are computed across each cell face using Roe's (ref. 16) flux-difference splitting (FDS). Spatial discretization is accomplished by a novel reconstruction process (ref. 17), which is based on an analytical formulation for computing solution gradients within tetrahedral cells. The solution is advanced to a steady state condition by an implicit backward-Euler time-stepping scheme (ref. 18). Flow turbulence effects are modeled by the Spalart-Allmaras (S-A) one-equation model (ref. 19), which can be coupled with a wall function to reduce the number of cells in the sublayer region of the boundary layer.

USM3D runs with multitasking on Cray vector processors, and on massively parallel processors such as the Origin 2000 and personal computer (PC) clusters. Memory is allocated dynamically. The code requires 175 eight-bit words per tetrahedron, and runs with individual processor times of 34 μsec/cell/cycle on a Cray-C90 and 230 μsec/cell/cycle on a single CPU of an Origin 2000.

Boundary Conditions

USM3D allows for an array of boundary conditions (BC) to suit many geometry and flow simulation needs. For the current investigation, the characteristic inflow and outflow BC was used on the far stream lateral planes. A full extrapolation BC was used along the

downstream far field boundary. The characteristic inflow and outflow BC was used on the far field inflow plane for subsonic freestream cases, and the freestream BC was used for supersonic freestream cases. Half of the FJEM and the FPVN geometry were modeled for this study, so the tangent flow BC was used along the symmetry plane. One quarter of the SCN geometry was used, so the tangent flow BC was used twice. The nozzle total pressure and injection total pressure was set using the engine exhaust BC.

Initial Conditions

Details on setting jet total pressure and temperature for the exhaust nozzle are shown in the USM3D online documentation[1]. Although directions for using the engine BC 102 specify the user to set p_{jet}=0.7143, each user must determine the value of this parameter for their desired flow conditions. For example, a low Mach number (M=0.2) nozzle inflow condition (upstream of the convergent section) was preferred in the present study to start the flow. Thus, equation 1 was used with M=0.2, resulting in a jet total pressure to jet static pressure ratio of 1.0283. Jet total pressure ($p_{t,jet}$) is normalized with γ for the USM3D input file, as shown in equation 2. Table 5 shows the values of $p_{o,jet}$ and p_{jet} at several NPR for each configuration. For M=0.2 nozzle inflow with NPR=5, $p_{o,jet}$=3.57 and p_{jet}=3.473. If, however, p_{jet} was set to 0.7143 as directed in the USM3D web site, the Mach number of the nozzle inflow would inappropriately be set at M=1.7. Freestream static temperature (T_∞) was determined with equation 3 and $T_{o,\infty}$=530°R. Jet total temperature ($T_{t,jet}$) is normalized with freestream static temperature for the USM3D input file, as shown in equation 4.

$$p_{o,jet}/p_{jet} = \{1 + (\gamma-1)/2 * M^2\}^{(\gamma/(\gamma-1))} \quad (1)$$

$$p_{o,jet} = p_{t,jet} / p / \gamma = \text{NPR} / \gamma \quad (2)$$

$$T_{o,\infty} / T_\infty = \{1 + (\gamma-1)/2 * M^2\} \quad (3)$$

$$T_{o,jet} = T_{t,jet} / T_\infty \quad (4)$$

[1]http://aaac.larc.nasa.gov/tsab/usm3d/usm3d_52_man.html

NPR	$p_{o,jet}$	p_{jet}	$T_{o,jet}$	T_∞ (°R)	M_∞
3.6	2.572	2.501	1.018	520.68	0.3
5.2	3.714	3.612	1.098	482.74	0.7
6	4.285	4.167	1.162	456.16	0.9
7.2	5.144	5.003	1.288	411.56	1.2
14.588	10.42	10.133	1.018	520.68	0.3
14.588	10.42	10.133	1.288	411.49	1.2

(a) Fluidic Jet Effects Model (FJEM).

NPR	$p_{o,jet}$	p_{jet}	$T_{o,jet}$	T_∞ (°R)	M_∞
5	3.571	3.473	1.162	455.00	0.9
5	3.571	3.473	1.288	410.458	1.2

(b) Supersonic Cruise Nozzle (SCN).

NPR	$p_{o,jet}$	p_{jet}	$T_{o,jet}$	T_∞ (°R)	M_∞
3	2.151	2.092	1.002	528.94	0.1
4.6	3.286	3.195	1.002	528.94	0.1
5	3.571	3.473	1.002	528.94	0.1
7	5	4.862	1.002	528.94	0.1
8.78	6.271	6.099	1.002	528.94	0.1
10	7.143	6.946	1.002	528.94	0.1

(c) Fluidic Pitch Thrust Vector Nozzle (FPVN).

Table 5. Engine conditions for input file.

Grid Study

The FJEM geometry was used for the grid study. USM3D often produces favorable results on external flows when used with the wall function (ref. 20). Therefore, the first set of simulations were run on the full nacelle grid with a wall function and a nondimensional first cell height of y^+=50. This boundary layer definition yielded solutions with an asymmetric pressure distribution along the upper and lower surfaces, as shown in figure 5. In order to investigate the pressure asymmetry, grids were generated to determine the best y^+ and number of layers for the boundary layer. Only the nozzle was simulated for this boundary layer investigation, in an effort to reduce cell count and improve solution output turnaround. The number of layers, generated with 3 tetrahedral cells per layer, defines the grid stretching rate within the boundary layer grid. The nozzle grids were generated with 8, 12, 16, and 20 nLayer and with y^+=0.5 or y^+=2.

Solutions were simulated on each grid with the overexpanded nozzle condition of NPR=3.6, to determine if the grid was adequate for predicting shock location. The two solid lines between 42.5 inches and 43.5 inches in figure 6(a) represent a pressure asymmetry along the top and bottom walls. This result indicates that 8 layers in the boundary layer grid yielded a grid stretching rate too great to adequately represent the flow. The grid stretching rate of the cells in the

boundary layer appeared to be sufficient with 16 layers, since there were negligible differences in wall pressure distributions whether 16 or 20 layers were used for either y^+=0.5 or y^+=2, see figures 6(a) and (b), respectively. Results indicate that the wall function with y^+=50 is completely inadequate for predicting the internal shock for this overexpanded nozzle condition, figure 6(c). The effect of y^+ on predicting wall pressure with 20 layers in the boundary layer is shown in figure 7. Identical wall pressure distributions for y^+=0.5 and y^+=2 indicate that a grid with y^+=2 is sufficient. Using a grid with a y^+=2 compared with y^+=0.5 would save 25,000 cells in the nozzle alone. The benefit would be further realized in a full nacelle and nozzle configuration. Therefore, the boundary layer for the full nacelle grids was defined with 16 layers and a y^+=2.

RESULTS

The focus of the present study was to assess the CFD system, *TetrUSS*, for use with propulsion applications. *TetrUSS* was used to simulate three nozzle configurations. For the present computations, the S-A one-equation turbulence model in the production version of USM3D was used. Results indicate that follow-on work with a two-equation turbulence model will be valuable.

Fluidic Jet Effects Model (FJEM)

The objective of the FJEM study in reference 5 was to understand the interaction between the external freestream flow and the internal nozzle flow, and determine the impact on fluidic thrust vectoring. Therefore, predicting pressure along the external boattail and the internal nozzle walls were both used as a means of evaluating USM3D for simulating the FJEM. Internal nozzle pressure distributions for several NPRs are shown in figure 8. The two CFD codes did not agree on shock location when the nozzle was operating at far off-design conditions (NPR=3.6). Based on experience running PAB3D with linear and nonlinear k-ε turbulence models, it is believed that S-A turbulence model is unable to predict the internal shock location in most off-design cases (refs. 3-5, 11-12).

The inability to predict the internal shock location may explain why USM3D did not predict the same pressure coefficient (C_p) distributions along the centerline of the boattail as PAB3D did for NPR<6, see figure 9. Historically, USM3D does well predicting external flows with S-A turbulence model, sometimes even using a wall function. However, the work in reference 5 uncovered an interaction between the internal and external flows. The internal shock moved further upstream with the influence of the external freestream compared with a static freestream. This interaction was greater at far off-design, overexpanded conditions than at the design NPR. So, if the code was unable to predict the correct internal shock location, it would also predict an incorrect flow field along the boattail. It is interesting that USM3D predicted the flow to expand to lower pressures on the boattail (fig. 9(a)), and the internal shock further upstream inside the nozzle (fig. 8(a)), compared to the PAB3D solution, as expected from the results in reference 5. PAB3D predicted the flow to expand further downstream inside the nozzle compared to USM3D, so the slightly larger plume deterred the flow from expanding as much along the boattail. For the case with a freestream Mach number of M=1.2 and nozzle condition of NPR=7.2, both codes predicted completely expanded internal flow. Therefore, the plume affected the external flow along the boattail the same for each code.

The normalized pressure distributions along internal nozzle walls and the pressure coefficient distributions along the boattail at the design condition, NPR=14.588, are shown in figures 8(e) and 9(e), respectively. Although both codes predicted complete internal expansion to the trailing edge, USM3D did not predict the same pressure recovery on the boattail that PAB3D predicted. USM3D predicted a shock near the trailing edge (x=42.5 inches), while PAB3D predicted a more gradual pressure recovery from x=41 inches.

Isolated Nacelle with Supersonic Cruise Nozzle (SCN)

The objective of the SCN study documented in reference 11 was to determine the effect of geometry variations on nozzle drag. Therefore, predicting pressure along the boattail was the primary interest for evaluating the ability of USM3D to predict the flow field. The nozzle was simulated at on-design conditions, NPR_D=5, with freestream Mach numbers of M=0.9 and M=1.2. Pressure coefficient distributions along the boattail for several grid densities are shown in figure 10. PAB3D predicted boattail pressure recovery very well using k-ε turbulence closure with nonlinear Reynolds stress modeling by Girimaji. USM3D did not predict the pressure recovery along the boattail with either external freestream, M=0.9 or M=1.2, using the one-equation turbulence model of S-A. For the M=0.9 simulation, USM3D predicted the general trend of flow expansion along the boattail and pressure recovery to C_p>0, although pressure recovery was delayed and higher values of C_p were predicted compared with experimentally measured and PAB3D results. Several grid densities were used in an effort to improve the USM3D prediction. However, there was little improvement in predicting pressure along the boattail with any of the grids. Therefore, higher order turbulence modeling, as used in the structured grid

simulation, is most likely required to improve the prediction.

Fluidic Pitch-Thrust-Vectoring Nozzle (FPVN)

The objective of the FPVN study documented in reference 12 was to predict internal nozzle performance and determine the effect of multiple injection slots on thrust vectoring performance. Predicting internal wall pressure distributions was used as a means of evaluating the ability of USM3D for simulating the FPVN configuration.

Normalized pressure distributions along the internal nozzle walls for simulations without thrust vectoring at NPR=3, 5, and 8 are shown in figures 11-13, respectively. At highly overexpanded conditions (NPR<8.78), USM3D predicted the shock location farther downstream than measured experimental data. There was a slight pressure asymmetry along the top and bottom walls for the NPR=3 simulation, see figure 11(a). Decreasing nondimensional first cell height from $y^+=1$ to $y^+=0.18$ eliminated the pressure asymmetry, but did nothing to improve the location of the shock, see figure 11(b). USM3D predicted wall pressure very well for the near design condition, NPR=8.

Normalized pressure distributions along internal nozzle walls, for the off-design thrust vectoring simulation at NPR=4.6, are shown in figure 14. Thrust vectoring is achieved with a fluidic injection secondary-to-primary total pressure ratio of SPR=0.7. USM3D predicted the shock location on both the upper and lower walls surprisingly well, considering the previous results predicted at off-design conditions. PAB3D-predicted and USM3D-predicted Mach contours along the symmetry plane for NPR=4.6, with SPR=0.7 for fluidic injection, are shown in figure 15(a) and 15(b), respectively. It is not surprising to see how well the solutions compared qualitatively after reviewing the internal pressure distributions.

Normalized pressure distributions along internal nozzle walls for the on-design condition, NPR=8.78, with a SPR=0.7 for fluidic thrust vectoring, are shown in figure 16. USM3D did an excellent job predicting the shock and pressurization upstream of the injection slot on the upper wall, figure 16(a). USM3D also predicted the slight increase in pressure downstream of the slot on the upper wall, as the flow reattached to the wall. The reattachment of flow was seen qualitatively in the Mach contours along the symmetry plane, in figure 17. Both codes predicted completely expanded flow along the lower divergent wall, figure 16(b).

It appears that although USM3D had difficulty predicting overexpanded flow in the nozzle, simulating fluidic injection for thrust vectoring was surprisingly less challenging. The flow separation at far off-design, overexpanded conditions was most likely a challenge for the 1-equation turbulence model. However, there was less flow separation inside the nozzle at overexpanded conditions, with the introduction of the secondary air stream for fluidic thrust vectoring. Thus, USM3D predicted a thrust vectoring simulation more accurately than an overexpanded condition with no fluidic injection.

CONCLUSIONS

1. Results indicate that USM3D provides accurate exhaust nozzle simulations at design NPR conditions. USM3D has difficulty predicting the shock location for overexpanded nozzle conditions.
2. The S-A 1-equation turbulence model appears inadequate for simulating the separation in the divergent section of the nozzle.
3. Simulating fluidic injection for thrust vectoring was surprisingly less challenging than simulating an off-design nozzle flow without fluidic injection. The introduction of the secondary air stream into the divergent section of the nozzle relieves the flow separation that is difficult for the code to predict with S-A turbulence modeling.
4. Grid generation is quick and efficient with VGRID. Grid generation of the Fluidic Jet Effects Model took 2 days with the unstructured grid generator, VGRID, compared with 30 days to generate the structured grid.

REFERENCES

(1) Pirzadeh, S.: *Three-Dimensional Unstructured Viscous Grids by the Advancing-Layers Method.* AIAA Journal, Vol. 34, No. 1, January 1996, pp. 43-49.

(2) Frink, N. T.; and Pirzadeh, S. Z.: *Tetrahedral Finite-Volume Solutions to the Navier-Stokes Equations on Complex Configurations.* Tenth International Conference on Finite Elements in Fluids, January 1998.

(3) Deere, K. A.; and Wing, D. J.: *PAB3D Simulations of a Nozzle with Fluidic Injection for Yaw-Thrust-Vector Control.* AIAA 98-3254, July 1998.

(4) Hunter, C. A.; and Deere, K. A.: *Computational Investigation of Fluidic Counterflow Thrust Vectoring.* AIAA 99-2669, June 1999.

(5) Deere, K. A.: *Computational Investigation of the Aerodynamic Effects on Fluidic Thrust Vectoring.* AIAA 2000-3598, July 2000.

(6) Pao, S. P.; and Abdol-Hamid, K. S.: *Numerical Simulation of Jet Aerodynamics Using Three-dimensional Navier-Stokes Method (PAB3D).* NASA TP-3596, September 1996.

(7) Krist, S. E.; Biedron, R. T.; and Rumsey, C. L.: *CFL3D User's Manual (Version 5.0).* NASA/TM-1998-208444, June 1998.

(8) Jespersen, D. C.; Pulliam, T. H.; and Buning, P. G.: *Recent Enhancements to OVERFLOW.* AIAA-97-0644, AIAA 35th Aerospace Sciences Meeting, January 1997.

(9) Vatsa, V. N.; Sanetrik. M. D.; and Parlette, E. B.: *A Multigrid Based Multiblock Flow Solver for Practical Aerodynamic Configurations.* Frontiers of Computational Fluid Dynamics, 1994, pp. 413-447.

(10) Wang, Q.; Massey, S. J.; Abdol-Hamid, K. S.; and Frink, N. T.: *Solving Navier-Stokes Equations with Advanced Turbulence Models on Three-Dimensional Unstructured Grids.* AIAA 99-0156, January 1999.

(11) Capone, F. J. and Deere, K. A.: *Transonic Investigation of Two-Dimensional Nozzles Designed for Supersonic Cruise.* AIAA 2001-3199, July 2001.

(12) Waithe, K. A.: *An Experimental and Computational Investigation of Multiple Injection Ports in a Convergent-Divergent Nozzle for Fluidic Thrust Vectoring.* Master of Science Thesis, May 2001.

(13) Frink, N. T.; Pirzadeh, S. Z.; Parikh, P.; Pandya, M. J.; and Bhat, M.: *The NASA Tetrahedral Unstructured Software System (TetrUSS).* The Aeronautical Journal, Volume 104, Number 1040, October 2000, pp. 491-499.

(14) Frink, N. T.: *Upwind scheme for solving the Euler equations on unstructured tetrahedral meshes.* AIAA Journal, Vol., No. 1, January 1992, pp. 70-77.

(15) Frink, N. T.: *Tetrahedral unstructured Navier-Stokes method for turbulent flows.* AIAA Journal, Vol. 36, No. 11, November 1998, pp. 1975-1982.

(16) Roe, P.: *Characteristic based schemes for the Euler equations.* Annual Review of Fluid Mechanics, Vol. 18, 1986, pp. 337-365.

(17) Frink, N. T.: *Recent progress toward a three-dimensional unstructured Navier-Stokes flow solver.* AIAA 94-0061, January 1994.

(18) Anderson, W.; and Bonhaus D.: *An implicit upwind algorithm for computing turbulent flows on unstructured grids.* Computers Fluids, Vol. 23, No. 1, 1994, pp. 1-21.

(19) Spalart P.; and Allmaras S. A.: *One-equation turbulence model for aerodynamic flows.* AIAA Paper 92-0439, January 1992.

(20) Frink, N. T.: *Assessment of an Unstructured-Grid Method for Predicting 3-D Turbulent Viscous Flows.* AIAA 96-0292, January 1996.

Acknowledgments

This work would not be possible without the efforts of many colleagues. As such, the authors would like to thank Dr. Paresh Parikh, NASA LaRC, for his consultation advice on unstructured-grid generation and for providing support during simulation development and analysis. The authors would also like to thank Dr. Neal T. Frink, NASA LaRC, for continued USM3D code improvements, for supplying the code description, and for his consultation expertise of USM3D. The authors also wish to thank Kenrick A. Waithe, Analytical Services & Materials, Inc. for providing experimental and structured-grid computational results for the FPVN configuration.

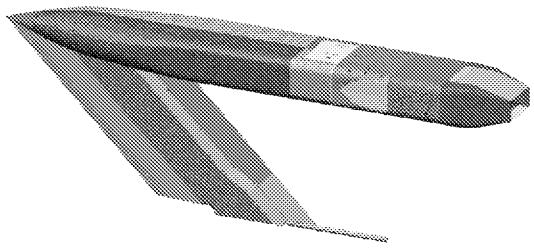

Figure 1. Isolated nacelle mounted on a strut (FJEM).

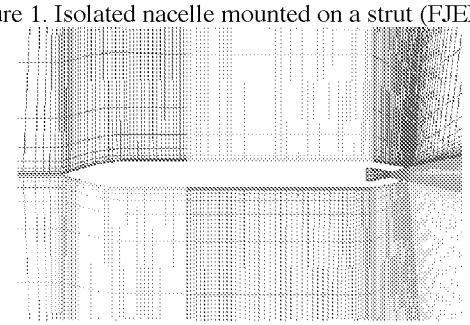

(a) Structured grid.

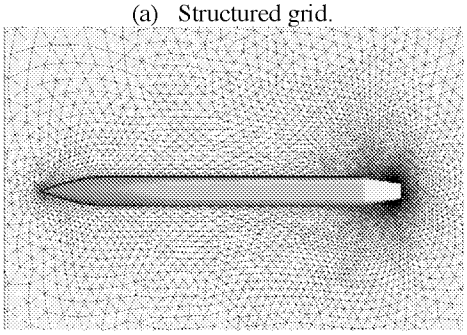

(b) Unstructured grid.

Figure 2. Symmetry plane, isolated nacelle and nozzle.

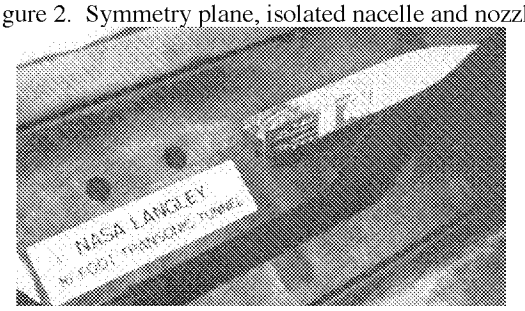

(a) Experimental model in 16-Foort Transonic Tunnel.

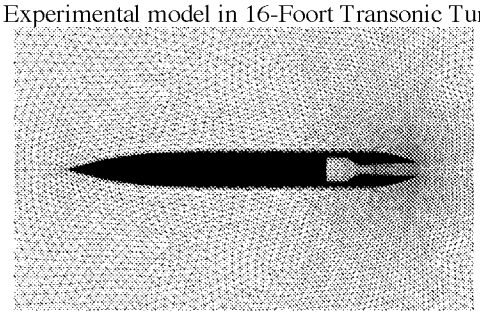

(b) Symmetry plane.

Figure 3. An isolated nacelle with a nozzle designed for the supersonic cruise civil transport.

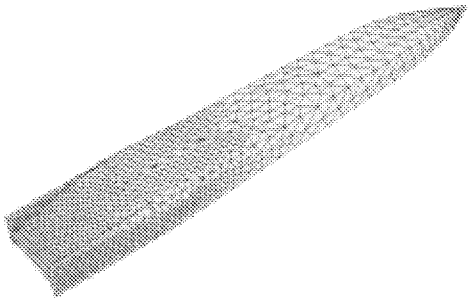

(c) Upper half of surface grid.

Figure 3. Continued

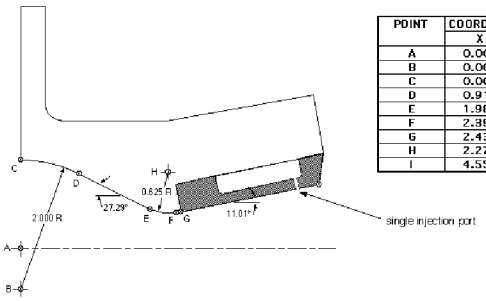

POINT	COORDINATES (IN.)	
	X	Y
A	0.000	0.000
B	0.000	-0.614
C	0.000	1.386
D	0.917	1.163
E	1.988	0.611
F	2.394	0.558
G	2.430	0.559
H	2.275	1.166
I	4.550	0.972

(a) Centerline plane, unstructured grid with plenum.

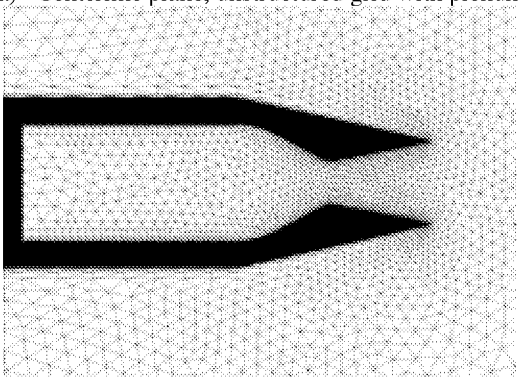

(b) Symmetry plane, unstructured grid without plenum.

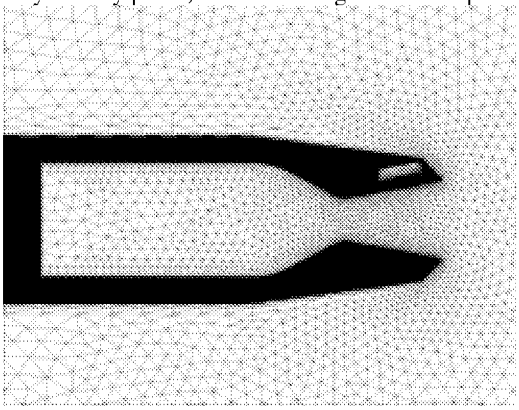

(c) Symmetry plane, unstructured grid with plenum.

Figure 4. Fluidic pitch-thrust-vectoring nozzle (FPVN).

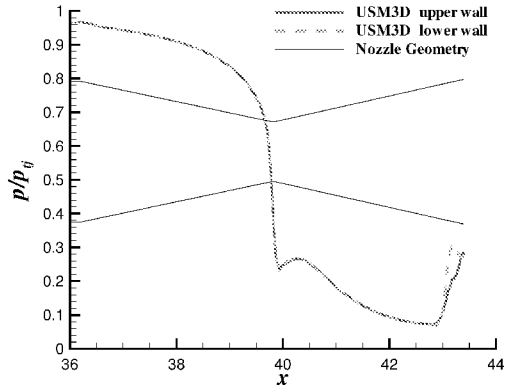

(a) Internal nozzle wall pressure distributions.

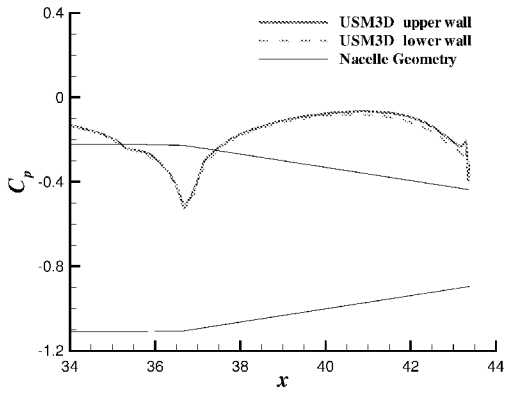

(b) External boattail pressure distributions.

Figure 5. Asymmetric pressure distributions with wall function and y^+=50, NPR=3.6, M=0.3 (FJEM).

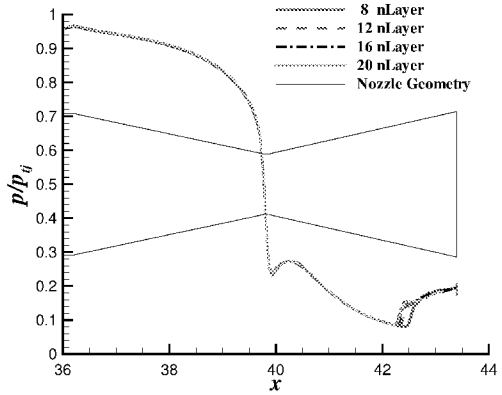

(b) $y^+ = 2$

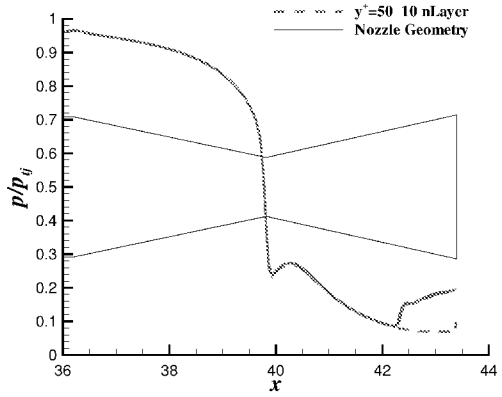

(c) Grid resolved boundary layer ($y^+ = 2$) simulation compared to wall function ($y^+ = 50$) simulation.

Figure 6. Continued.

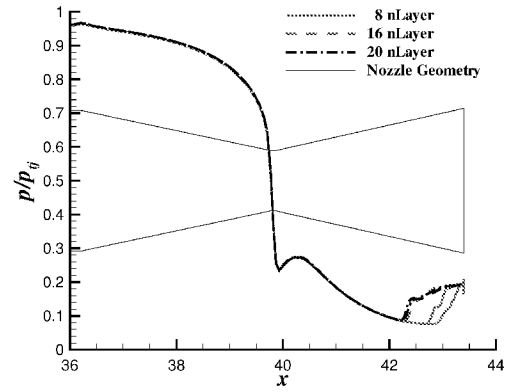

(a) $y^+ = 0.5$

Figure 6. The effect of number of cell layers in the boundary layer on nozzle wall pressure, NPR=3.6.

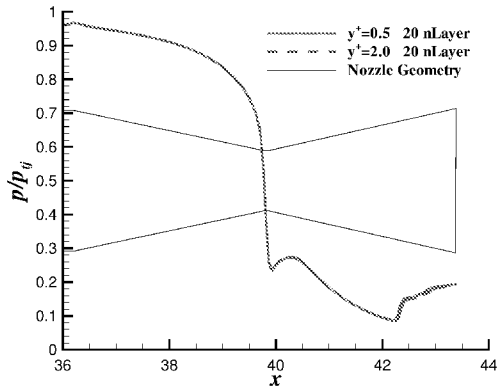

Figure 7. The effect of y^+ on nozzle wall pressures, NPR=3.6.

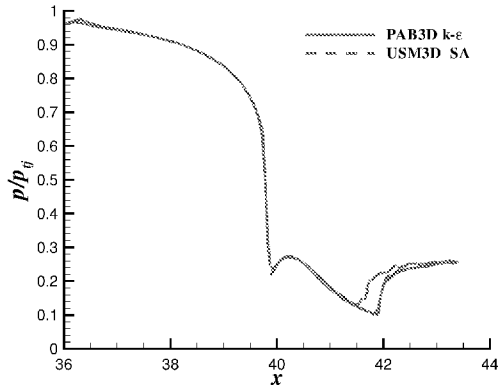

(a) M=0.3, NPR=3.6

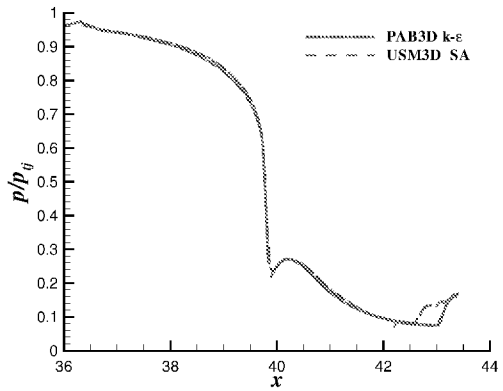

(b) M=0.7, NPR=5

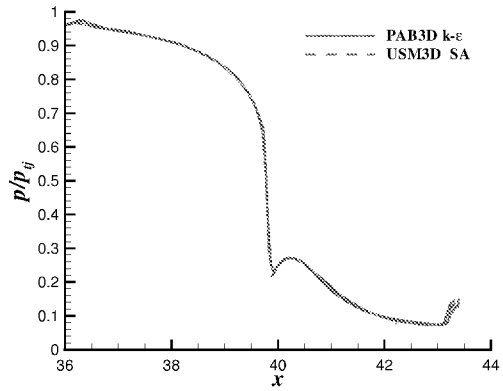

(c) M=0.9, NPR=6

Figure 8. Internal nozzle pressure distributions for several NPR, (FJEM).

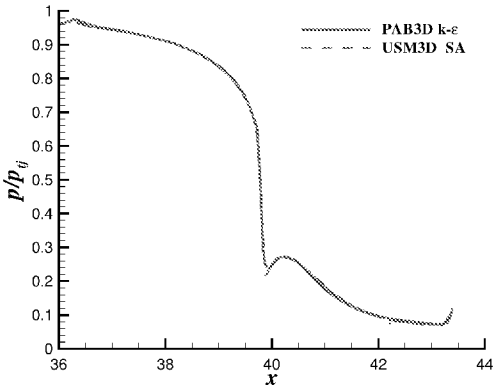

(d) M=1.2, NPR=7.2

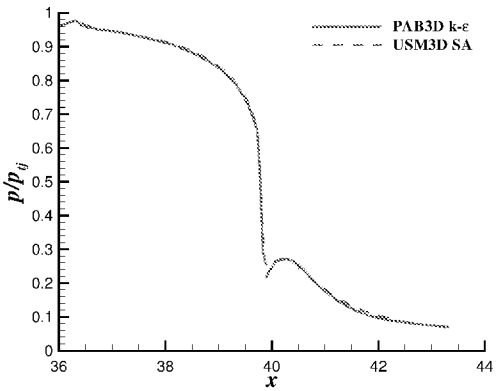

(e) M=1.2, NPR=14.588

Figure 8. Continued.

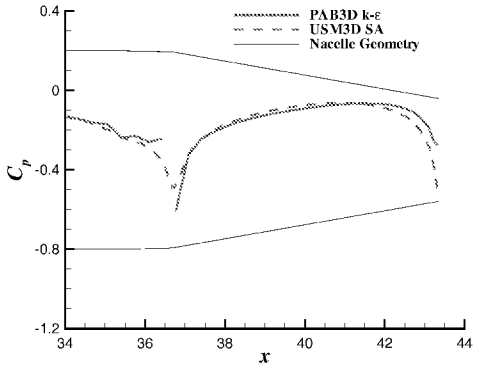

(a) M=0.3, NPR=3.6

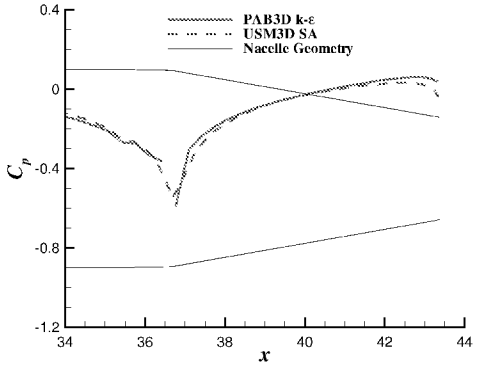

(b) M=0.7, NPR=5

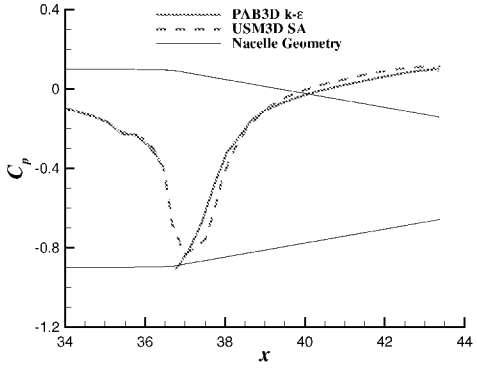

(c) M=0.9, NPR=6

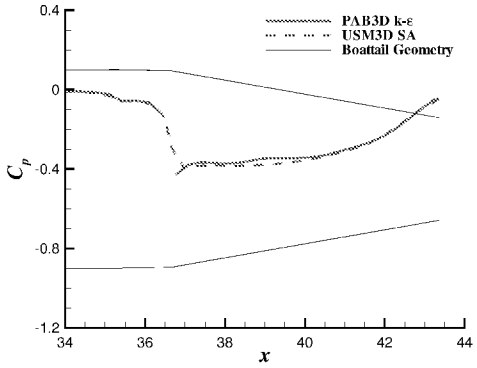

(d) M=1.2, NPR=7.2

Figure 9. Pressure coefficient distributions along boattail for several Mach numbers, (FJEM).

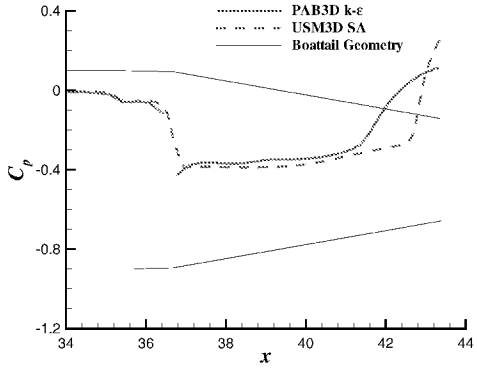

(e) M=1.2, NPR=14.588

Figure 9. Continued.

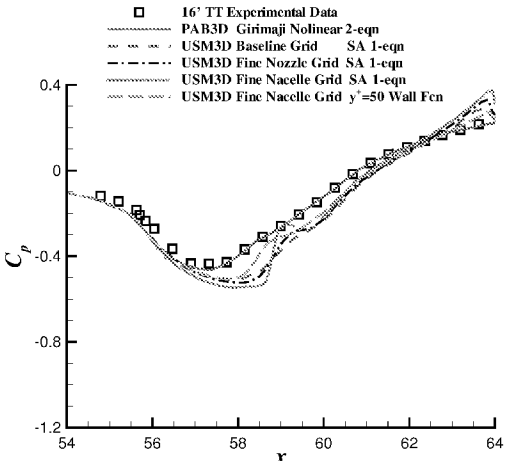

(a) M=0.9, NPR=5

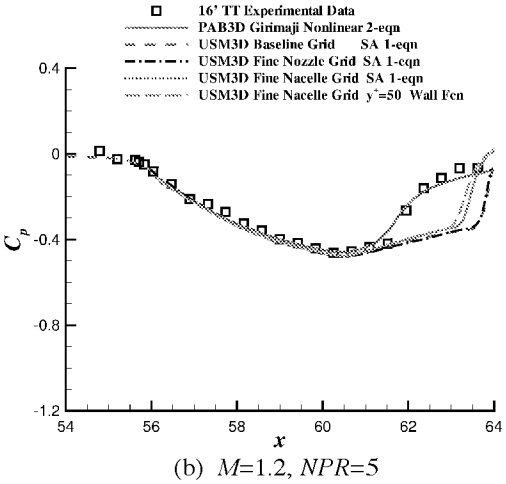

(b) M=1.2, NPR=5

Figure 10. Pressure coefficient distributions along boattail for several grid densities, (SCN).

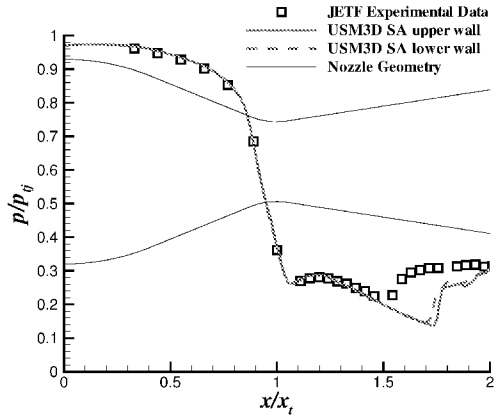

(a) y^+ = 1, 15 nLayer

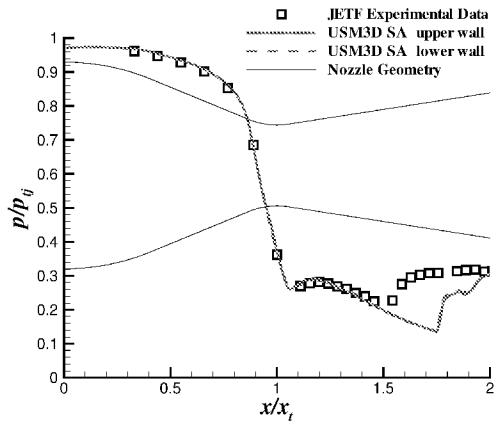

(b) y^+ = 0.18, 18 nLayer

Figure 11. Effect of y^+ on pressure distribution, NPR=3, M=0.1, (FPVN).

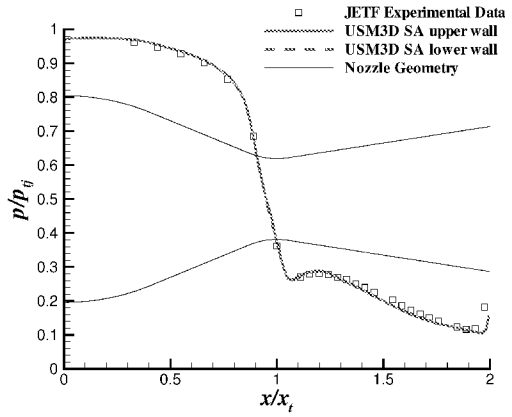

Figure 12. Comparison of pressure distribution for NPR=5, M=0.1, y^+ = 0.18, 18 nLayer, (FPVN).

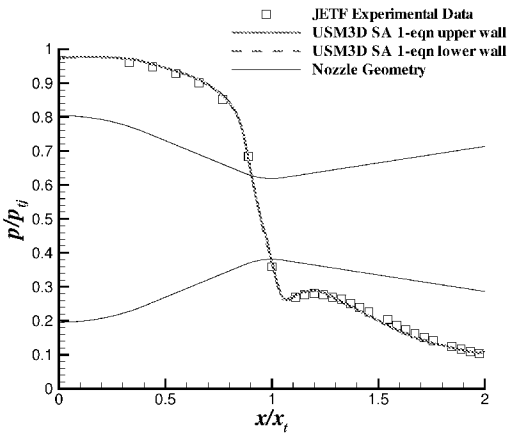

Figure 13. Comparison of pressure distribution for NPR=8, M=0.1, y^+ = 0.18, 18 nLayer, (FPVN).

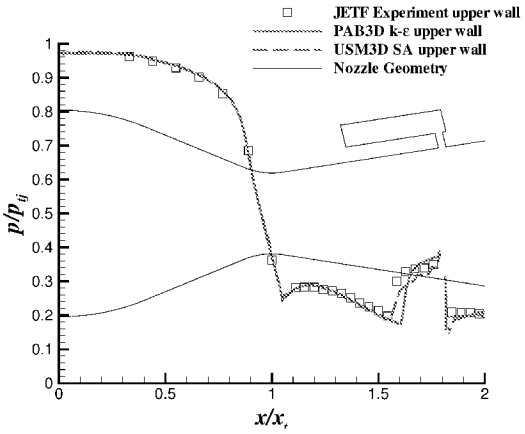

(a) Upper nozzle wall.

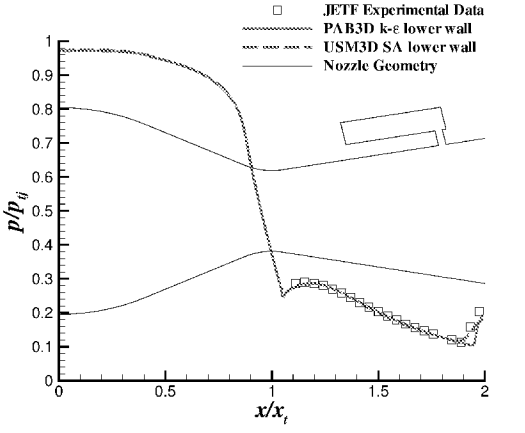

(b) Lower nozzle wall.

Figure 14. Normalized pressure along internal nozzle walls, NPR=4.6 with SPR=0.7 for fluidic injection, y^+ = 1, 17 nLayer, (FPVN).

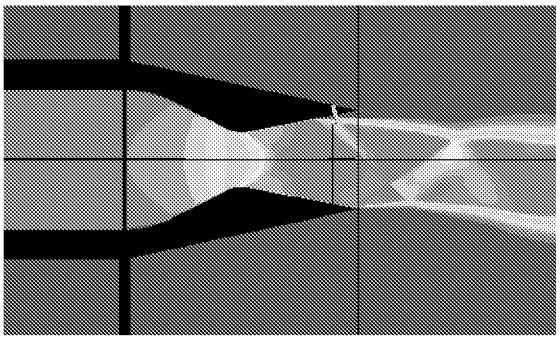

(a) PAB3D

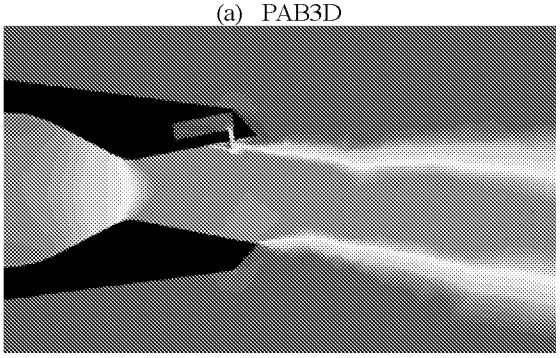

(b) USM3D

Figure 15. Mach contours along the symmetry plane, NPR=4.6 with SPR=0.7 for fluidic injection, (FPVN).

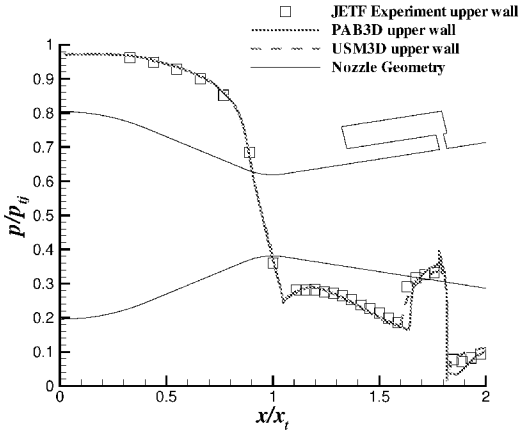

(a) Upper nozzle wall.

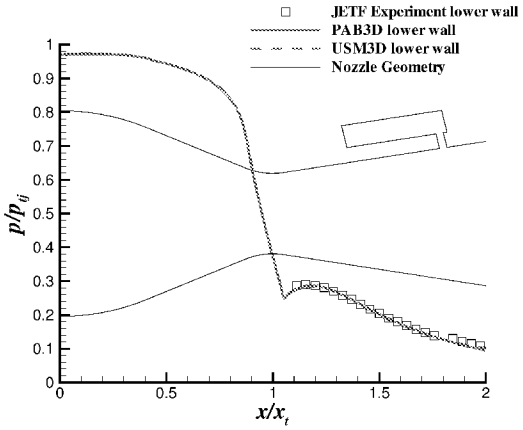

(b) Lower nozzle wall.

Figure 16. Normalized pressure along internal nozzle walls, NPR=8.78 with SPR=0.7 for fluidic injection, y^+ = 1, 17 nLayer, (FPVN).

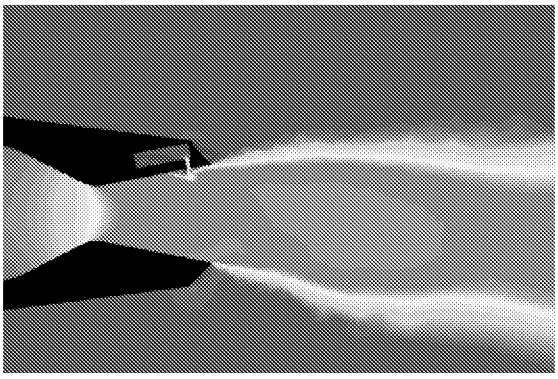

Figure 17. Mach contours along the symmetry plane, NPR=8.78 with SPR=0.7 for fluidic injection, (FPVN).